

Supplementary information

Titanium dioxide-supported non-precious metal oxygen reduction electrocatalysts

Gang Wu,^{*a} Mark A. Nelson,^a Nathan H. Mack,^b Shuguo Ma,^c Praveen Sekhar,^a
Fernando H. Garzon^a and Piotr Zelenay^{*a}

^aMaterials Physics & Applications Division and ^bChemistry Division, Los Alamos National Laboratory, Los Alamos, NM 87545, USA.

E-mail: wugang@lanl.gov; zelenay@lanl.gov

^cDepartment of Chemical Engineering, University of South Carolina, Columbia, SC 29208, USA

1. Materials synthesis and characterization

Catalyst synthesis: Commercially available TiO₂, with the particle size ranging from 50 to 150 nm and in the B.E.T. surface area from 50 to 100 m²/g, was first treated in 0.5 M HCl solution for 24 hours to remove impurities. In a typical approach to the synthesis of the PANI-Fe-TiO₂ catalyst, 2.0 mL aniline was first dispersed in 0.5 M HCl solution. The solution was kept below 10°C while the oxidant (ammonium peroxydisulfate, (NH₄)₂S₂O₈, APS) and transition metal precursors (FeCl₃) were added. The solution was stirred for three hours to allow aniline to fully polymerize and form polyaniline (PANI). Then 1.0 g of HCl-treated TiO₂ was mixed with the PANI. After constant mixing for 24 hours, the suspension containing TiO₂, polymer, and Fe species was vacuum-dried using a rotary evaporator. After ball-milling the dry powders for 24 hours, the subsequent heat treatment was performed at temperatures ranging from 800 to 1000°C in an inert atmosphere of nitrogen gas for one hour. The heat-treated sample was then pre-leached in 0.5 M H₂SO₄ (typically using 100 mL of solution per 0.1 g of the catalyst powder) at 80°C for 8 hours to remove unstable and inactive species from the catalyst and then thoroughly washed in de-ionized water. In the final step, the catalyst was heat-treated again under identical conditions to the first heat treatment to reduce the oxygen-containing functional groups on the catalyst surface, thereby enhancing hydrophobicity. The product was a PANI-Fe-TiO₂ non-precious metal catalyst. In order to explore the roles of nitrogen, iron and TiO₂ in ORR catalysis, the performance of various catalysts synthesized in this study has been compared to that of the TiO₂, heat-treated PANI-coated TiO₂ (denoted as PANI-TiO₂), and PANI-Fe supported on carbon black, Ketjenblack EC-300J (PANI-Fe-C). These samples were subjected to identical heat-treatment and chemical post-treatment steps.

Rotating disk electrode (RDE) and rotating ring-disk electrode (RRDE) measurements:

ORR activity was electrochemically evaluated with rotating disk electrode (RDE) and catalyst selectivity for the four-electron reduction of oxygen (hydrogen peroxide yield) was determined with rotating-ring-disk electrode (RRDE). RDE/RRDE measurements were performed using a CHI Electrochemical Station (Model 750b) in a conventional three-electrode cell. To avoid any potential contamination of non-precious metal catalyst by platinum, all experiments were carried out with a graphite rod as the counter electrode. A Ag/AgCl electrode in 3.0 M NaCl (0.232 V *vs.* RHE at 25°C) was used as a reference electrode. All measured potentials were later converted to the RHE scale. Performance data reported in this paper was recorded at a total catalyst loading of 0.6 mg cm⁻² for non-precious samples in 0.5 M H₂SO₄ at a rotating disk speed of 900 rpm and room temperature. In RDE tests, ORR steady-state polarization curves were recorded with a potential step of 0.03 V and a period time of 30 s from 1.0 to 0.1 V using a negative-going scan. For comparison, ORR activity of 20 wt% E-TEK Pt/C catalyst with a loading of 20 μg cm⁻² was recorded from 0.1 to 1.0 V using a positive-going scan in 0.1 M HClO₄ solution to avoid specific adsorption of the bisulfate anion. In RRDE experiments, the Pt ring was activated by potential cycling in N₂-saturated 0.5 M H₂SO₄ solution from 0 to 1.4 V at a scan rate of 50 mV s⁻¹ for 10 min. The ring potential was set to 1.2 V to determine H₂O₂ yield.

Fuel cell testing: PANI-derived non-precious metal catalysts were tested at the fuel cell cathode to evaluate their activity and durability under PEFC operating conditions. Catalyst inks were prepared by ultrasonically mixing catalyst powders with Nafion® solution for four hours. The inks were then applied to the gas diffusion layer (GDL, ELAT LT 1400W, E-TEK) by successive brush-painting in layers until the cathode catalyst loading reached 4 mg cm⁻². The Nafion® content in the dry catalyst was controlled around 35 wt%. A commercially-available Pt-catalyzed cloth GDL (E-TEK, 0.25 mg_{Pt} cm⁻²) was used as the anode. The thickness of carbon black- and TiO₂-based catalyst layers was determined by x-ray micro-tomography technique. In good agreement with the difference in density of the two support materials, the catalyst layer of carbon black-supported catalyst is around 60 μm while that of the TiO₂-supported catalyst is around 40 μm.

The cathode and anode were hot-pressed onto the opposite sides of a Nafion® 212 membrane. The geometric area of the MEA was 5.0 cm². Fuel cell testing was carried out in a single cell with serpentine anode/cathode flow channels. Pure hydrogen and oxygen humidified at 85°C were supplied to the anode and cathode at a flow rate of 200 and 400 mL min⁻¹, respectively. Both electrodes were maintained at the same backpressure of 2.8 bar (about 40 psi absolute pressure at the Los Alamos altitude). Fuel cell polarization plots were recorded using fuel cell test stations (Fuel Cell Technologies, Inc.). The reference

polarization fuel cell plot with a Pt/C catalysts at the cathode was recorded at a cell temperature of 80°C and backpressures of 2.8 (H₂)-2.8 bar (air).

Physical characterization: Elemental quantification and specie analysis using X-ray photoelectron spectroscopy (XPS) were performed on an ESCA 210 and MICROLAB 310D spectrometer. Mid-infrared spectra were recorded on a Nicolet 670 FTIR spectrometer on KBr pellets. The sample morphology was characterized by scanning electron microscopy (SEM) on an FEI Quanta 400 ESEM instrument. High-resolution transmission electron microscopy (HR-TEM) images were taken on a JEOL 3000F microscope operating at 300 kV. The crystallinity of various samples was determined by X-ray diffraction (XRD) using a Bruker AXS D8 Advance diffractometer with Cu K α radiation.

2. Elemental analysis by XPS

Elemental quantification of samples treated at different temperatures was performed using XPS (data shown in **Table 1**). Fewer Fe species were found in the surface layer of PANI-Fe-TiO₂ catalyst than in the carbon-supported PANI-Fe catalysts after an analogous acidic leach step. As a result of PANI carbonization, the carbon content in the surface layers increased with the heat-treatment temperature up to 86.4 at% in the sample treated at 1000°C. Generally, the decline of oxygen and nitrogen content from 800 to 1000°C was determined, except for the 900°C-treated sample that exhibited slightly higher N content. The sulfur in the XPS images is associated with FeS formed during the heat-treatment step *via* reaction(s) between FeCl₃ (Fe precursor) and (NH₄)₂S₂O₈ (oxidant used for aniline polymerization). While the subsequent acid leach leads to the removal of a vast majority of FeS aggregates from PANI-Fe-TiO₂, trace amounts of the sulfide are still detected by XPS. Our recent experiments involving sulfur-free PANI-derived catalysts indicate that sulfur is unlikely to directly participate in the ORR active site. The details are included in the following upcoming publication: Z. Ding, C. Johnston and P. Zelenay, *ECS Trans.*, 2010, in press.

Table 1. Elemental quantification analysis of PANI-Fe-TiO₂ catalysts

Heat-treatment temperature, °C	Atomic concentration, %					
	C 1s	O 1s	N 1s	S 2p	Ti 2p	Fe 2p
800	80.8	10.7	4.4	0.7	2.2	1.2
900	83.9	7.4	5.1	0.3	2.6	0.7
1000	86.4	8.0	2.5	0.6	1.8	0.7

3. TEM images

HR-TEM images of heat-treated PANI-TiO₂ system in the absence of iron are shown in **Figure S1**. *In-situ* carbonized PANI (light contrast) can be seen next to the TiO₂ particles. In spite of intrinsically low electronic conductivity of the TiO₂ support itself, the catalyst conductivity overall is sufficient without the use of any additional dopants. The graphitized carbon layer next to the non-carbon TiO₂ particles after the catalyst synthesis is apparently continuous enough to eliminate the need for significant electronic conductivity in the TiO₂ support.

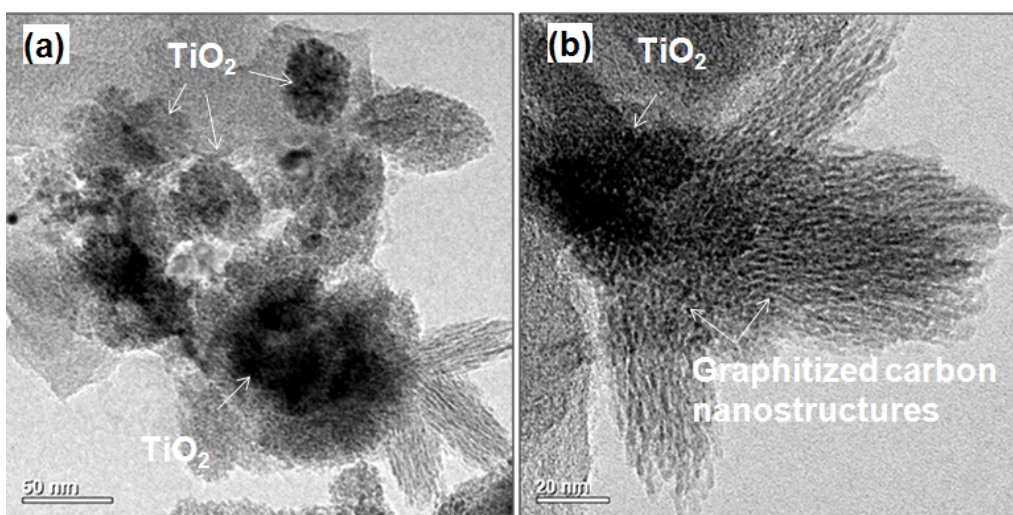


Figure S1. TEM images of heat-treated PANI-TiO₂ system at two magnifications.

4. Durability testing of carbon-supported reference catalyst (PANI-Fe-C)

The durability of the PANI-Fe-C non-precious metal catalyst was examined under voltammetric cycling conditions in the potential range from 0.6 to 1.0 V (**Figure S2**) using 50 mV/s scan rate, following accelerated stress test (AST) protocol suggested by U.S. DOE for fuel cell cathode catalysts based on precious metals. We adopted those conditions in the absence of a protocol for non-precious metal catalysts, which is yet to be developed. In N₂-saturated 0.5 M H₂SO₄, only 10 mV loss in half-wave potential was observed with PANI-Fe-C catalyst after 10,000 cycles (Figure S2a). Voltammetric cycling in O₂-saturated electrolyte resulted in an 80-mV negative shift in E_{1/2} in RDE testing (Figure S2b).

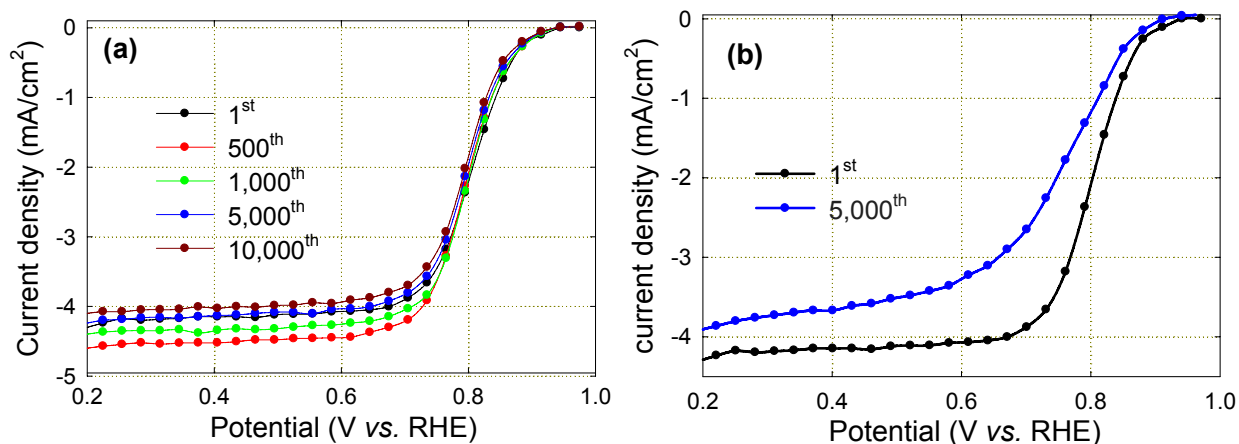


Figure S2. Durability test of PANI-Fe-C by cycling catalyst in 0.5 M H₂SO₄: (a) N₂-saturated and (b) O₂-saturated.

5. FT-IR spectra

FT-IR spectra show that the benzene (1100 cm⁻¹) and quinone-type (1420 cm⁻¹) structures in the main PANI chain break into smaller species, such as C=N, between 400 and 600°C (**Figure S3**). There is no obvious change in the FT-IR spectra following the heat treatment at temperatures higher than 600°C.

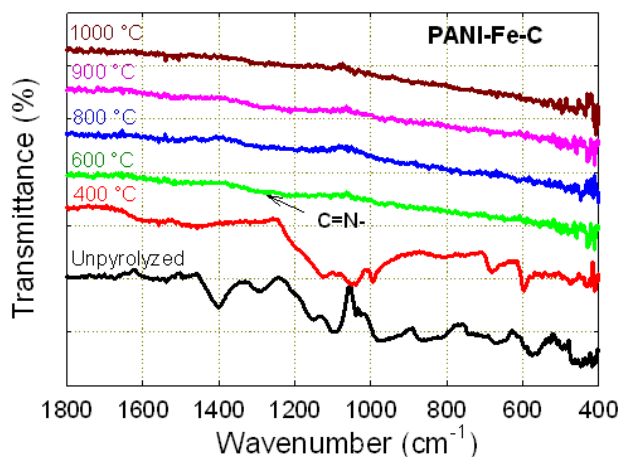


Figure S3. Effect of heat-treatment temperature on FT-IR spectra of PANI-Fe-C catalysts.

6. SEM study of PANI-Fe-TiO₂ catalyst

SEM images of PANI-Fe-TiO₂ catalysts at different synthesis stages are shown in **Figure S4**. The particle size of TiO₂ is around 50-150 nm (Figure S4a). These particles become invisible following *in-situ* polymerization of PANI with well-dispersed nanofiber morphology, ~40 nm

in diameter and ~ 200 nm in length (Figure S4b). Based on the FT-IR analysis before and after the heat treatment, the PANI structure decomposes during the heat treatment. The graphitized nanofibers are directly converted from PANI fibers with thinner diameters (Figure S4c). The iron-associated metallic aggregates that incorporate into the nanofiber network nearly disappear after the chemical pre-leaching with sulfuric acid (Figure S4d). Noticeably, while the first heat-treatment step is required for the formation of the active sites and inducing ORR activity, the removal of unstable phases from the porous catalyst surface in the acid leaching step leads to further improvement in the performance. More active sites are likely being exposed and higher surface area with increased mass transfer is achieved.

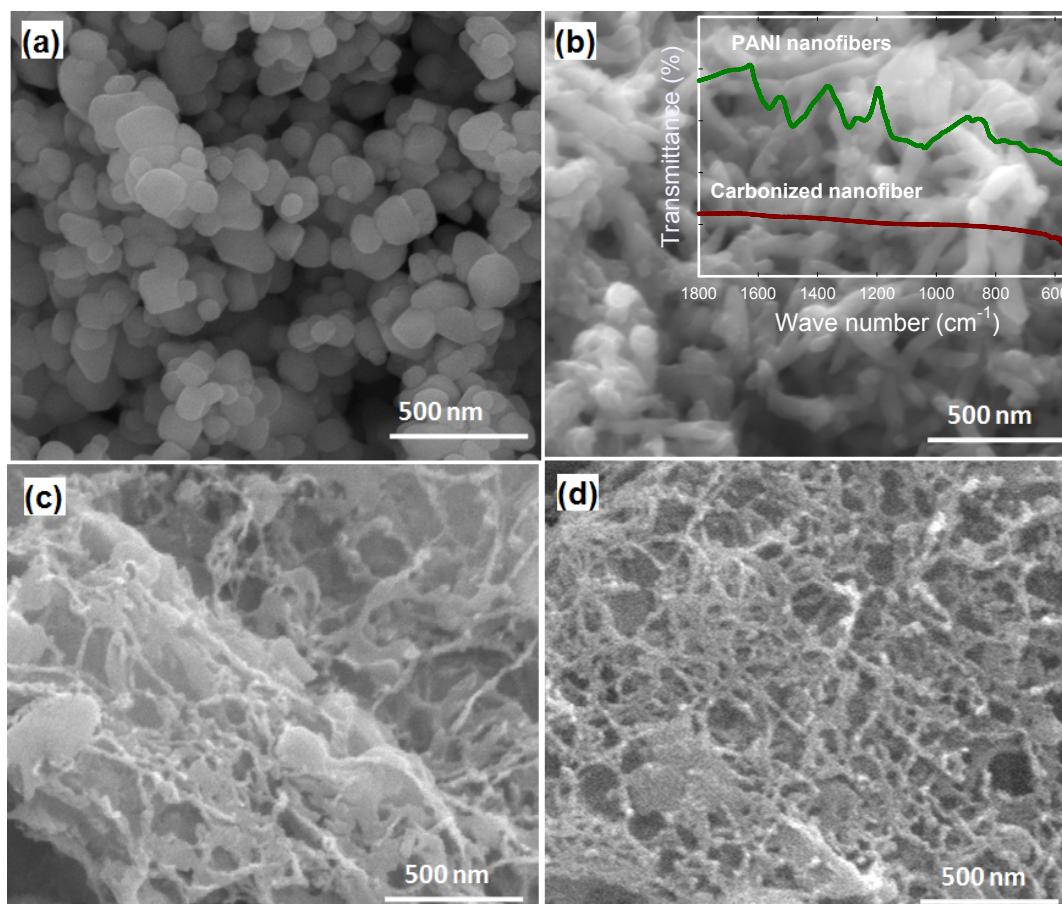


Figure S4 SEM images of PANI-Fe-TiO₂ catalyst at different synthesis stages: (a) as-received TiO₂ particles, (b) *in-situ* polymerized PANI with Fe species and TiO₂ particles, (c) PANI-Fe-TiO₂ catalyst after heat treatment, and (d) PANI-Fe-TiO₂ catalyst after heat treatment and acid leach.

7. XRD patterns

XRD was used to analyze each sample heat-treated in the experimental temperature range (800-1000°C), as shown in **Figure S5**. The XRD results indicate that heat treatment yields FeS as a dominant phase in the PANI-derived catalysts. That phase originates from the use of

(NH₄)₂S₂O₈ for polymerizing aniline (see above). Unlike for PANI-Fe-C, the subsequent acid leach leads to virtually complete removal of FeS aggregates from the PANI-Fe-TiO₂ samples. More effective leaching of FeS from PANI-Fe-TiO₂ than PANI-Fe-C may be associated with lower porosity of the TiO₂-supported catalyst and could result in an improvement in the ORR activity and durability. It is worth noting that a small amount of rutile TiO₂ phase converted from anatase begins to appear at 900°C and becomes the dominant phase at 1000°C. This is presumably one of the reasons for the maximum in ORR activity observed following the heat treatment at 900°C. Likely, the use of a heat-treatment temperature higher than 900°C has a negative effect on the overall surface area and porosity, as well as on the density of active sites, following a collapse of the graphitized carbon structures.

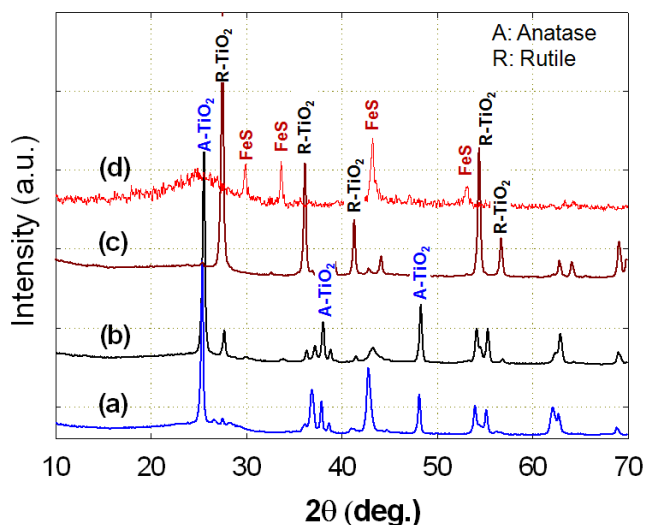


Figure S5. XRD patterns for PANI-Fe-TiO₂ catalyst after heat treatment at (a) 800°C, (b) 900°C, and (c) 1000°C, and (d) for PANI-Fe-C catalyst after heat treatment at 900°C and acid leach.